Nanopore size distribution heterogeneity of organic-rich shale reservoirs using multifractal analysis and its influence on porosity-permeability variation

Gaoyuan Yan [a, b], Zhengyuan Qin [c*], Stuart Marsh [c], Stephen Grebby [c], Yi Mou [d,e], Lijuan Song [a], Chenchen Zhang [a]

[a] School of Architectural Construction, Jiangsu Vocational Institute of Architectural Technology, Xuzhou, 221116, China

[b] Key Laboratory of Coalbed Methane Resource & Reservoir Formation Process, Ministry of Education, China University of Mining and Technology, Xuzhou 221008, China

[c] Nottingham Geospatial Institute, Faculty of Engineering, University of Nottingham, NG7 2TU, UK

[d] Mine Safety Technology Branch of China Coal Research Institute, Beijing 100013, P. R. China

[e] State Key Laboratory of Coal Mining and Clean Utilization (China Coal Research Institute), Beijing 100013, P. R. China

Abstract: The shale nano-pore size (diameter <100nm) distribution heterogeneity (SNDH) is one of the important factors affecting gas production. However, quantitative analysis of the SNDH and the applicability of single and multi-fractal model needs to be further studied. Here, based on low temperature liquid nitrogen and carbon dioxide tests of organic rich shale in Qinshui Basin, multifractal dimension variation of micro-pores (< 2 nm) and meso-pores (2–100 nm) are studied, and the multifractal factors that affect the distribution of nano-pores are determined. Additionally, the differences between single fractal and multifractal results are compared. Based on this, dynamic variation of porosity and permeability under the constraints of nano-pore structure is discussed from the perspective of multifractal variation. The results of this study are as follows: 1) pore size distribution of micro-pores and meso-macro-pores in shale samples exhibit typical multifractal behavior. The overall distribution heterogeneity of meso-macro-pores is mainly affected by the distribution of pores in the low value area of pore volume (LAPV), while the overall distribution heterogeneity of micro-pores is affected by the distribution of high value area of pore volume. The multifractal parameters and influencing factors of micro-pores and meso-macro-pores are clearly different. 2) The single fractal dimension D_2 calculated using the Frenkel-Halsey-Hill

model has a negative correlation with the multifractal parameters, implying that the distribution heterogeneity of the LAPV gradually decreases with the increase of the D_2 value, indicating that the physical meaning of the two models is obviously different. 3) The pore distribution heterogeneity affects permeability variation and diffusion process of shale reservoir. With the increase of the multifractal dimension of meso-macro-pores, the damage effect of stress on permeability is stronger. The more heterogeneous the micro-pore size distribution is, the smaller the "modification effect" of stress on the diffusion coefficient.

Key words: shale reservoirs; pore structure heterogeneity; permeability variation; diffusion; fractal dimension

0 Introduction

As an unconventional natural gas reservoir, nano-pores are widely developed in shale reservoir. The adsorption pore surface adsorbs methane molecules in the form of physical adsorption, which controls adsorption characteristics and affects the gas bearing content of the shale reservoir. Accordingly, pore structure has become an important factor in determining the production potential of shale gas [1-3].

At present, experimental techniques such as photoelectric observation, gas adsorption and fluid intrusion, as well as three-dimensional structure reconstruction methods, are widely used in the study of unconventional reservoir pore-fracture structure [4-9]. Among them, fluid injection has become the most common technique. Along with high pressure mercury injection (HPMI) tests, low pressure nitrogen adsorption (LPN_2 GA) tests have become an effective technology to characterize shale nano-pore structure [10-11]. However, given the large molecular diameter (0.36 nm) and the accuracy of the instrument, it is difficult to accurately characterize the microporous structure [10, 12-17].

In contrast to nitrogen, carbon dioxide has a low molecular diameter and strong adsorption capacity and it can enter into pores of diameter 0.3–1.5 nm at 273.15 K. Therefore, comprehensive utilization of both liquid nitrogen and carbon dioxide adsorption tests can help realize the full-scale pore structure of shale reservoirs [12-13]. In addition, since the storage and migration of shale methane is closely related to the pores and surfaces of unconventional reservoirs with self-similarity, the fractal dimension value obtained from LPN_2 GA test has become an effective physical parameter to quantitatively describe the nano-pore structure heterogeneity of shale reservoirs [14-17]. This combination of tests and analysis therefore provides a basis for quantitative description of shale pore structure heterogeneity.

However, the above model can only describe shale nanopore size distribution heterogeneity (SNDH) simply by a single fractal dimension. For shale reservoirs with strong heterogeneity, the pore size distribution (PSD) curve usually fluctuates or jumps randomly, and different pore size intervals may have different types of self-similarity, and so it is difficult to fully characterize pore homogeneity with a single fractal dimension [18-19]. To overcome this, a multifractal approach can be adopted, in which a fractal body is divided into small regions with different singularities. The advantage of studying the fractal characteristics of these different regions is that it enables the detailed structure to be understood hierarchically and allows the multiple characteristics of pore size distribution of reservoirs to be analyzed based on HPMI, LPN_2 GA and low field nuclear magnetic resonance (LF-NMR) test data. In this context, Vidal-Vazquez et al. [20] studied the multifractal characteristics of soil by using LPN_2 GA data, and concluded that this parameter has a clear relationship with the basic properties. Liu et al. [21-22] analyzed the multifractal parameters of shale samples and indicated that shale nano-pores have a better multi-fractal variation. Li et al. [23] and Song et al. [24] analyzed the multifractal variation of tectonic coal using HPMI tests, and showed that the multifractal parameters have a clear relationship with the degree of structural development. Zhang et al. [25-26] compared the variation of single and multifractal parameters through LPN_2 GA and NMR T_2 spectra respectively, and concluded that the multifractal model has good applicability for describing the heterogeneity of tight sandstone pore size distribution.

While studies on multifractal features have expanded from the macroscopic to the microscopic pore scale, there are still some problems that need to be addressed. Compared with other types of reservoirs, there are very few studies on multifractal analysis of nanopores in shale reservoirs, and the influencing factors on multifractal parameters need to be clarified. Moreover, micropores are the main pores for methane adsorption. There are relatively few studies on the NPSH in this pore component and in particular, the variation of multifractal characteristics needs to be further studied. In general, it is the above two factors that restrict the accurate quantitative characterization of shale nanopore structure.

With this in mind, this study aim to analyze the multifractal characteristics of micropores and meso-macropores of shale samples by using LPN_2/CO_2 GA of organic shale in Qinshui Basin, and the factors influencing the nano-pore size distribution. The differences between single fractal and multifractal results are also compared. Based on this, dynamic variation of porosity and permeability under the constraints of nanopore structure will be discussed from the perspective of multifractal variation. Overall, the results of the study are anticipated to provide a theoretical basis for the quantitative evaluation of shale reservoirs pore heterogeneity.

1 Experimental sample and methods

1.1 Sample collection and basic analysis

The shale samples were obtained from Well 1 in Qinshui Basin, which is located at the eastern edge of the central part of the basin, with a total thickness of 162.67m. A total of 12 samples were collected from black shale from top to bottom [16]. Basic tests such as TOC, whole-rock mineral composition and $R_{o,\,max}$ are performed on fresh shale samples. For a detailed description of these experimental test procedures, please refer to Yan et al. [16].

1.2 Experimental methods

After measuring TOC, field emission scanning electron microscopy (FE-SEM) and LPN_2/CO_2 GA tests were performed on the samples in sequence (the reader is referred to Yan et al. [16] for detailed information), and the overburden porosity and diffusion coefficient tests were performed on a selection of four representative samples. Information on the sample tests is shown in Table 1.

Different permeability was measured by pressure-sensitive testing using an AP-608 Automated Permeameter-Porosimeter [25]. The experimental method is based on the non-steady state pressure drop method and the experimental gas comprised highpurity nitrogen. During the measurement process, the gas pressure difference between the two ends of the core holder is set to 0.7 MPa to form an initial attenuation pressure pulse between V_1 volume and V_2 volume. The instrument automatically tests the pressure attenuation and calculates the pulse attenuation permeability values of different confine pressure and pore pressure points. The effective stress was continuously increased to 5, 10, 15 and 20 MPa by changing the confine pressure (the gas pressure was always maintained at 1 MPa). Each pressure point was tested for 30 min to remove the effects of pressurization time and total volume change, and the two pressure points were maintained at intervals of 30 seconds.

1.3 Multi-fractal theories

The multifractal characteristics of adsorption data (reflecting pore size distribution heterogeneity) under different test methods can be studied using the box counting method. When analyzing the volume probability of T_2 spectrum in the interval [a, b], the scale and measurement need to be determined.

The scale and measure expressions are, respectively

$$\varepsilon = 2^{-k} L \tag{1}$$

$$\overline{\Delta n_i} = \frac{\Delta n_i - \Delta n_{\min}}{\sum_{i=1}^{N} (\Delta n_i - \Delta n_{\min})} \tag{2}$$

where the relative pressure is divided into several boxes of equal length for gas adsorption, and the box size is represented by ε. The analysis interval of liquid nitrogen adsorption data ranges from 0 to 0.99 MPa, while the analysis interval of carbon dioxide adsorption data is 0.01–0.03 MPa. Therefore, the corresponding value of ε differs [26].

In the case of scale variation, the water distribution probability in the interval [A, B] satisfies

$$p_i(\varepsilon) \sim \varepsilon^{-a_i} \tag{3}$$

where $P_i(\varepsilon)$ is the mass probability function of the i^{th} box, which is used to quantitatively analyze the distribution of gas adsorption capacity in each box; a_i reflects the local singular intensity, and a high value represents the smoothness or regularity of the data. Conversely, the smaller the value, the greater degree of data variation or the stronger the irregularity will be. a_i is related to the area and reflects the probability of the area.

After the singularity index is obtained, the object under investigation is divided into a series of subsets, so that the small units in each subset have the same singularity index. Then, the number of units in this subset is calculated and the relationship between the number of units and the scale is defined as

$$N_a(\varepsilon) \sim \varepsilon^{-f(a)}, \varepsilon \to 0 \qquad (4)$$

where $f(a)$ is the multifractal spectrum, which is the fractal dimension of the subset with the same singularity index. The curve formed by a and $f(a)$ is called the multifractal singular spectrum, which is used to investigate the uneven distribution of the gas adsorption amount, thereby giving more structural information than the single fractal. If the investigated object is multifractal, $f(a)$ generally represents a unimodal image.

The expressions of singularity index a and $f(a)$ are respectively [23]

$$a(q) \infty \frac{\sum_{i=1}^{N(\varepsilon)} [u_i(q,\varepsilon) \lg \varepsilon]}{\lg \varepsilon} \qquad (5)$$

$$f(a) \infty \frac{\sum_{i=1}^{N(\varepsilon)} [u_i(q,\varepsilon) \lg u_i(q,\varepsilon)]}{\lg \varepsilon} \qquad (6)$$

$$u_i(q,\varepsilon) = \frac{p_i^{\,q}(\varepsilon)}{\sum_{i=1}^{N(\varepsilon)} p_i^{\,q}(\varepsilon)} \qquad (7)$$

where q is the order of the statistical matrix. When q>>1, large concentration information or high degree of aggregation is amplified; when q<<1, small concentration information or low degree of aggregation is amplified. In this study, q is an integer between -10 and 10, and the step size is 1. a and $f(a)$ can be obtained by linear regression of the above two formulas.

The $f(a)$ parameters include a_{min}, a_{max}, a_0, a_0- a_{max}, a_{min}- a_0 and A. The symmetry of the singularity spectrum can be expressed as $A= (a_{min}- a_0) / (a_0-a_{max})$. The left oblique shape indicates that the measured values are affected by large fluctuations, while the right oblique shape indicates that the measured values are affected by small fluctuations [24, 27, 28].

Here a~$f(a)$ is a set of basic language describing local features of multifractals, called the multifractal spectrum. The other set is $q \sim D(q)$, which is introduced from the perspective of information theory and is termed the generalized fractal dimension. The parameter D_q includes D_{-10}, D_{10}, D_0, D_1, D_2, D_{-10}-D_{10}, D_0-D_{10}, and D_{-10}-D_0. D_{-10} is influenced by the lowest probability measure areas, whereas D_{10} is influenced by the highest probability measure areas. D_1 is the information dimension and characterizes the degree of disorder in the PSD. A value of D_1 of 1 represents a uniform pore size distribution. D_2 is the correlation dimension and characterizes the association between the measures contained in the multifractal set. D_0-D_{10} and D_{-10}-D_0 are the amplitudes of the right and left branches of D_q, which represent the heterogeneity of the high and low probability measure areas, respectively. For the detailed derivation process, please refer to Zhang et al. [26].

2 Results and discussion

2.1 Multifractal parameter variation of meso-macropore using LPN_2 GA

2.1.1 Multifractal parameter variation

According to the LPN_2 GA data for the representative sample W1, the double logarithm diagram of the partition function $x(q,\varepsilon)$ and the size length ε is calculated using Eqs. 2–7 (Fig. 1a). The results show that lg[$u_i(q, \varepsilon)$] value has an obvious linear relationship with lg(ε), and Fig. 1b shows that $i(q)$ increases strictly monotonically with the increase of the value of q, which shows that the pore size distribution obtained from the LPN_2 GA data has multifractal characteristics. When the q value is less than 0, there is a negative correlation between lg[ui(q, ε)] and lg(ε). When the q value is larger than 0, there is a positive correlation between lg[ui(q, ε)] and lg(ε). This shows that the nano-pore size distribution in those shale samples is concentrated and the pore distribution interval is smaller [26].

By combining with Eqs. 5–7, generalized and singular fractal dimension spectra of meso-macropores of all the samples are obtained (Fig. 1c and d). The results show that the q~$D(q)$ spectra of all the shale samples are “anti-s-type”, which is another typical feature of shale pore size distribution in line with multifractals. The spectral lines can effectively characterize the pore size distribution complexity at different pore size, which can then reveal the local differences in the whole pore diameter.

To investigate the multifractal variation of all samples, generalized fractal parameters of all the samples were calculated (Table 1). As outlined in Section 1.3, the spectrum width D_{-10}- D_{10} represents the variation degree of overall SNDH. D_{-10}- D_{10} of all the samples is 0.69–1.26, which shows that the pore size distribution difference among those samples is relatively large. The D_{-10}-D_0 value is greater than that of D_0-D_{10}, indicating that SNDH in the LAPV was more complex than that in the HAPV. In addition, it should be noted that the D_0-D_{10} values of some samples are 0.57, which indicates that SNDH in the HAPV is consistent, and the overall SNDH is controlled by the pore distribution in the LAPV.

It can be seen from Fig. 2a that there is no obvious correlation between D_{-10} and D_{10}, which is related to the consistent values of the two parameters amongst the samples. In contrast to the results shown in Fig. 2a, D_{-10}-D_0 and D_0-D_{10} are positively correlated (Fig. 2b), although there is no clear linear relationship between them. Fig. 2c shows that D_{-10}-D_{10} increases linearly with the increase of D_{-10}-D_0. Compared with D_{-10}-D_0, the linear relationship between D_0-D_{10} and D_{-10}-D_{10} is not remarkable. Considering the two factors, the overall SNDH is affected by the LAPV.

2.1.2 Influencing factors of multifractal parameters

Based on the data in Table 1, the influencing factors of nanopore multifractal parameters are examined by integrating the shale maturity, mineral composition, organic matter content and pore structure parameters (Fig. 3). Figs.3a–c show that two fractal parameters D_{-10}-D_0 and D_0-D_{10} are weakly correlated with variation in $R_{o,max}$ and brittle mineral content. Compared with Fig. 3d and 3e, it can be concluded that the fractal parameter has a strong correlation with the pore structure, which is manifested through the D_{-10}-D_0 value decreasing as the pore volume increases, implying that the SNDH of LAPV is weakened. The reason for this is that the increase of total pore volume, accompanied by the decrease of mesopore volume and increase of micro-pore volume, which causes the pore interval in this range change from HAPV to LAPV, results in the distribution of low-value area of pore volume tending to be uniform, subsequently leading to the decrease of D_{-10}-D_0 value [26].

2.1.3 Pore size distribution heterogeneity obtained from different fractal models

By using Table 4 in Yan et al. [16], the correlation of fractal dimension calculated by different fractal models is compared. The above study shows that D_1 calculated using the Frenkel-Halsey-Hill (FHH) model reflects the SNDH of pores >10 nm, and D_2 reflects the SNDH of pores between 2 and 10 nm [26]. Fig. 4 shows that there is no clear correlation between the single fractal parameter D_1 and the two multifractal parameters, while the single fractal parameter D_2 and the multifractal parameters show a clear negative correlation that implies that the SNDH of LAPV is weakened. Zhu et al. showed that D_2 (relative pressure corresponding to 0–0.5) characterize adsorption pore surface heterogeneity, and D_1 (relative pressure corresponding to 0.5–1) can reveal the adsorption pore volume heterogeneity [27]. The increase of the D_2 value shows that pore surface heterogeneity increases, and the D_{-10}-D_0 value decreases shows that the SNDH of LAPV is weakened. In conclusion, the fractal dimension values calculated using the two fractal models are different. The result shows that the multifractal model represents SNDH in different pore size intervals, and the calculated values are relative values. The single fractal model represents the overall heterogeneity of the pore distribution, which its absolute value is calculated.

2.2 Multifractal parameter variation of micro-pore by using LPCO_2 GA

2.2.1 Multifractal parameter variation

According to the LPCO_2 GA data of the representative sample W1, the double logarithm diagram of the partition function $x(q,\varepsilon)$ and the size length ε is calculated (Fig. 5a). The results show that lg[$u_i(q, \varepsilon)$] value has an obvious linear relationship between lg(ε), and Fig. 5b shows that $i(q)$ increases strictly monotonically with the increase of q value, which indicates that the pore size distribution obtained from LPCO_2 GA data has multifractal characteristics. When the q value is less than 0, there is a negative correlation between lg[$u_i(q, \varepsilon)$] and lg(ε). When q value is greater than 0, a positive correlation is observed between lg[u_i(q, ε)] and lg(ε). This shows that the micro-pore size distribution in those shale samples is concentrated and the pore distribution interval is smaller.

Fig. 5c shows that the $q \sim D(q)$ spectrum of all shale samples is "Anti-S" type, which is also typical feature of multifractal distribution of shale pore-fracture system. The spectrum can effectively represent the complexity of PSDH in different pore stage. Compared with Fig. 1c it can be seen that the singular spectral width of highly mature shale samples is different, and the width of the left branch is larger, which indicates that PSDH is stronger and is related to the HAPV.

Table 3 shows that D_{-10}-D_0 value is less than D_0-D_{10}, meaning that the SNDH of HAPV is stronger than that of LAPV in micro-pores, which implies that the HAPV controls the micro-pore size distribution heterogeneity. Compared with Fig. 3, the LAPV in the range of 2–100nm controls SNDH within that pore range, indicating that there are obvious differences in the overall distribution of pores <2 nm and 2–100 nm. The D_{-0}-D_1 value of all the samples is 0.50–0.72, which is less than that of the value of 2–1200 nm pores, indicating that the overall distribution of pores of 2–100 nm is more complex.

An analysis of micro-pore multifractal parameters shows that D_{-10} and D_{10} have an obvious linear positive correlation, showing that the minimum and maximum pore volume distribution characteristics are synchronized (Fig. 6a). As shown in Fig. 6b, D_{-10}-D_0 decrease linearly with the increase of D_0-D_{10}, indicating the distribution heterogeneity of LAPV decreases with the increased HAPV heterogeneity. Fig. 6c shows that D_{-10}-D_{10} and D_{-10}-D_0 as well as D_0-D_{10} are linearly negatively and positively correlated, respectively, and the linear fit of the latter is significantly higher than that of the former. In summary, the heterogeneity of full-scale pore distribution is controlled by HAPV.

2.2.2 Influencing factors of multifractal parameters

The influencing factors of the micro-pore multifractal parameters are examined by integrating the shale maturity, mineral composition, organic matter content and pore structure parameters (Fig. 7). The results show that the micro-pore single fractal parameters D_{-10}-D_0 and D_0-D_{10} have weak correlations with various influencing factors. Compared to Fig. 3b, Fig. 7b shows that there is no obvious relationship between the two fractal parameters and the micro-pore volume. The reason being that the pore size range corresponding to the low/high pore volume area is not constant. Yan et al. [16] found that there are three peak intervals in the micro-pore distribution of all of the analysed shale samples, which are 0.38 nm, 0.5 nm and 0.85 nm. With the variation in micro-pore volume, the three-peaks of pores corresponding to the high pore volume area are relatively complicated, so the correlation among the two multifractal parameters and pore volume is weak. Zhang et al. [26] analyzed the micro-pore multifractal characteristics of middle and high rank coal samples from western Guizhou and eastern Yunnan, which showed that the micropore [0.72, 0.94] distribution variation was an important interval leading to variation in the micro-pore multifractal. Therefore, the focus of further research should be on exploring the micro-pore interval that affects the distribution of high value area of micropores.

Fig.8 shows that there is no correlation between the multifractal parameters of micro-pores and meso-pores, which also explains the strong heterogeneity of shale pore size distribution.

2.3 Dynamic variation of porosity and permeability under the influence of pore size distribution heterogeneity

Four representative samples, capturing the variation in the physical characteristics within the reservoir, were selected for further analysis based on their initial porosity, permeability and pore distribution. Fig. 9 shows that the initial permeability of all the samples is different, with the initial permeability of samples W7 and W9 both exceeding 0.1 mD while sample W1 reaches 0.29 mD. The overburden porosity results are also shown in Fig. 9. The results shows that the permeability of all samples decreased exponentially when the effective stress increased from 0 to 25 MPa, and the maximum R^2 reached 0.99.

In addition, permeability varies in stages with the increase in effective stress. When the effective stress is less than 15 MPa, permeability (including pore volume) decreases rapidly with the increase in stress, and the permeability is in the stage of rapid decline with the average decline of all the samples in the region of 86%. However, when the effective stress is greater than 15 MPa, the permeability is in a slow decline stage and is fairly stable. Initially, the pore volume has not been compressed and so the compressible space is large. The pore space therefore has high compressibility, which leads to the rapid decline of coal permeability during this early phase of applying stress. With the continuous increase in stress, the compressible space of meso-macro-pores is reduced the compressibility coefficient decreases, which results in the coal permeability being stable during this stage.

Fig. 9 shows that the permeability loss rate of all samples is between 0.76 and 0.98. Among them, the permeability of sample W1 is the most sensitive to pressure, and the permeability loss rate can reach 98%. In the other three samples, the macro-pores are not developed. As a result, the compressible space in the high stress stage is provided by micro-pores. However, the meso-pores influence the permeability variation, so the permeability loss rate is relatively higher.

According to the multifractal parameters and permeability damage rate of samples, D_{-10}-D_0 and D_{-10}-D_{10} has obvious linear positive correlation with permeability damage rate (Fig. 10). According to above two parameters, the relationship between D_0-D_{10} and permeability damage rate is not obvious, which implies that the stronger pore heterogeneity, the more obvious the damage effect of stress on permeability is. This conclusion is also consistent with the previous results.

Table 4 shows that with the exception of sample W10, the initial diffusion coefficients of samples are 2.14–2.41×10^{-6} cm^2/s and are fairly uniform. The diffusion coefficient increases with the increase of confining stress, which indicates that the pressure has a positive effect on the diffusion coefficient. In order to systematically explain the influence of pressure on the diffusion coefficient, the diffusion coefficient variation coefficient D_{20}/ D_{10} is introduced to quantitatively characterize the diffusion coefficient variation under pressure. The calculation results indicates that the value is between 2.34 and 8.21. Relevant literature shows that micro-pores play an important role in controlling methane diffusion coefficient. In Section 2.2, the relationship between the multifractal parameters and diffusion coefficient variation is discussed (Fig. 11). It indicates that the variation rate of diffusion coefficient decreases with the increase in the multifractal parameters, indicating that the stronger the heterogeneity of pore distribution, the weaker the "transformation effect" of stress on the diffusion coefficient (Table 4) [28-30].

3 Conclusions

According to low temperature liquid nitrogen and carbon dioxide tests (LPN_2/CO_2 GA) of organic rich shale in Qinshui Basin, the multifractal dimension variation of micro-pores (<2 nm) and mesopores (2–100 nm) was studied, and the multifractal factors that affect the distribution of nanopores determined. In addition, the differences between single fractal and multifractal results were compared. Based on this, the dynamic variation of porosity and permeability under the constraints of nanopore structure were discussed from the perspective of multifractal variation. The conclusions are as follows:

1) The distribution of nanopores in organic rich shale is a typical multifractal feature. However, there are obvious differences in the multifractal parameters and influencing factors between micropores and mesopores.

2) The SNDH in the HAPV of 2–100nm in shale samples tends to be consistent, and the overall SNDH is controlled by the SNDH in the LAPV. The SNDH in the LAPV is affected by the distribution of pores with diameter within 2 and 10 nm.

3) The single fractal dimension D_2 calculated using the FHH model has a negative correlation with the multifractal parameters, which implies that the distribution heterogeneity of the LAPV gradually decreases with the increase of D_2, indicating that the physical meaning of the two models is clearly different.

4) In contrast to meso-macropores, the heterogeneity of the micro-pore size distribution is controlled by HAPV, and the correlation between the multifractal variation and pore volume is weak. Moreover, there is no correlation between micro-pore and mesoporous multifractal parameters, which shows the strong heterogeneity of shale pore distribution.

5) Multifractal variation of pores controls the porosity and permeability variation and diffusion process of shale reservoirs. D_{-10}-D_0 and D_{-10}-D_{10} has an obvious linear positive correlation with permeability variation rate, indicating that the stronger the pore heterogeneity, the greater the damage effect of confining stress on permeability.

Also, the stronger the heterogeneity of the micro-pore size distribution, the weaker the "reconstruction effect" of stress on the diffusion coefficient.

Acknowledgements

This work is supported by Key Laboratory of Coalbed Methane Resources and Reservoir Formation Process of the Ministry of Education (China University of Mining and Technology) (No. 2019-006).

References

[1] Dong J, Hsu J, Wu W, et al. Stress-dependence of the permeability and porosity of sandstone and shale from TCDP Hole-A[J]. International Journal of Rock Mechanics and Mining Sciences. 2010, 47(7): 1141-1157.

[2] Bao Y, Ju Y, Yin Z, et al. Influence of reservoir properties on the methane adsorption capacity and fractal features of coal and shale in the upper Permian coal measures of the South Sichuan coalfield, China[J]. Energy Exploration & Exploitation. 2020, 38(1): 57-78.

[3] Mosher K, He J, Liu Y, et al. Molecular simulation of methane adsorption in micro- and mesoporous carbons with applications to coal and gas shale systems[J]. International Journal of Coal Geology. 2013, 109-110: 36-44.

[4] Wang Y, Zhu Y, Chen S, et al. Characteristics of the Nanoscale Pore Structure in Northwestern Hunan Shale Gas Reservoirs Using Field Emission Scanning Electron Microscopy, High-Pressure Mercury Intrusion, and Gas Adsorption[J]. Energy & Fuels. 2014, 28(2): 945-955.

[5] Bao Y, Ju Y, Huang H, et al. Potential and Constraints of Biogenic Methane Generation from Coals and Mudstones from Huaibei Coalfield, Eastern China[J]. Energy & Fuels. 2018, 33(1): 287-295.

[6] Zhou L, Kang Z. Fractal characterization of pores in shales using NMR: A case study from the Lower Cambrian Niutitang Formation in the Middle Yangtze Platform, Southwest China[J]. Journal of Natural Gas Science and Engineering. 2016, 35: 860-872.

[7] Yang R, He S, Yi J, et al. Nano-scale pore structure and fractal dimension of organic-rich Wufeng-Longmaxi shale from Jiaoshiba area, Sichuan Basin: Investigations using FE-SEM, gas adsorption and helium pycnometry[J]. Marine and Petroleum Geology. 2016, 70: 27-45.

[8] Habina I, Radzik N, Topór T, et al. Insight into oil and gas-shales compounds signatures in low field 1H NMR and its application in porosity evaluation[J]. Microporous and Mesoporous

Materials. 2017, 252: 37-49.
[9] Zhang J, Wei C, Ju W, et al. Stress sensitivity characterization and heterogeneous variation of the pore-fracture system in middle-high rank coals reservoir based on NMR experiments[J]. Fuel. 2019, 238: 331-344.
[10] Mastalerz M, Hampton L, Drobniak A, et al. Significance of analytical particle size in low-pressure N_2 and CO_2 adsorption of coal and shale[J]. International Journal of Coal Geology. 2017, 178: 122-131.
[11] Aljamaan H, Al Ismail M, Kovscek A R. Experimental investigation and Grand Canonical Monte Carlo simulation of gas shale adsorption from the macro to the nano scale[J]. Journal of Natural Gas Science and Engineering. 2017, 48: 119-137.
[12] Zhang, J.; Wei, C.; Yan, G.; Lu, G., Structural and fractal characterization of adsorption pores of middle–high rank coal reservoirs in western Yunnan and eastern Guizhou: An experimental study of coals from the Panguan syncline and Laochang anticline. Energy Exploration & Exploitation 2019, 37, (1), 251-272.
[13] Jiang J, Yang W, Cheng Y, et al. Pore structure characterization of coal particles via MIP, N_2 and CO_2 adsorption: Effect of coalification on nanopores evolution[J]. Powder Technology. 2019, 354: 136-148.
[14] Hu J, Tang S, Zhang S. Investigation of pore structure and fractal characteristics of the Lower Silurian Longmaxi shales in western Hunan and Hubei Provinces in China[J]. Journal of Natural Gas Science and Engineering. 2016, 28: 522-535.
[15] Shao X, Pang X, Li Q, et al. Pore structure and fractal characteristics of organic-rich shales: A case study of the lower Silurian Longmaxi shales in the Sichuan Basin, SW China[J]. Marine and Petroleum Geology. 2017, 80: 192-202.
[16] Yan G, Wei C, Song Y, et al. Pore characteristics of organic-rich shale in the Carboniferous-Permian coal-bearing strata in Qinshui Basin[J]. Energy Exploration & Exploitation. 2017, 35(5): 645-662.
[17] Guo X, Huang Z, Zhao L, et al. Pore structure and multi-fractal analysis of tight sandstone using MIP, NMR and NMRC methods: A case study from the Kuqa depression, China[J]. Journal of Petroleum Science and Engineering. 2019, 178: 544-558.
[18] Zhang J, Hu Y. Comparative evaluation of pore structure heterogeneity in Low-Permeability

tight sandstones using different fractal models based on NMR technology: A case study of Benxi Formation in the Central Ordos Basin[J]. Energy Fuels. 2020, 34(11): 13924-13942.

[19] Zhang J, Wei C, Luo J. Volume and surface distribution heterogeneity of nano-pore in coal samples by CO_2 and N_2 adsorption experiments[J]. Acta Geological Sinaca (English Edition). 2020.

[20] Vidal-Vázquez E, Paz-Ferreiro J. Multifractal characteristics of nitrogen adsorption isotherms from tropical soils[J]. Soil Science. 2012, 177(2): 120-130.

[21] Liu K, Ostadhassan M, Kong L. Multifractal characteristics of Longmaxi Shale pore structures by N_2 adsorption: A model comparison[J]. Journal of Petroleum Science and Engineering. 2018, 168: 330-341.

[22] Liu K, Ostadhassan M, Zou J, et al. Multifractal analysis of gas adsorption isotherms for pore structure characterization of the Bakken Shale[J]. Fuel. 2018, 219: 296-311.

[23] Li W, Liu H, Song X. Multifractal analysis of Hg pore size distributions of tectonically deformed coals[J]. International Journal of Coal Geology. 2015, 144-145: 138-152.

[24] Yu S, Bo J, Pei S, et al. Matrix compression and multifractal characterization for tectonically deformed coals by Hg porosimetry[J]. Fuel. 2018, 211: 661-675.

[25] Zhang J, Wei C, Zhao J, et al. Comparative evaluation of the compressibility of middle and high rank coals by different experimental methods[J]. Fuel. 2019, 245: 39-51.

[26] Zhang J, Wei C, Chu X, et al. Multifractal Analysis in Characterizing Adsorption Pore Heterogeneity of Middle- and High-Rank Coal Reservoirs[J]. ACS Omega. 2020, 5(31): 19385-19401.

[27] Zhu J, Liu J, Yang Y, et al. Fractal characteristics of pore structures in 13 coal specimens: Relationship among fractal dimension, pore structure parameter, and slurry ability of coal[J]. Fuel Processing Technology. 2016, 149: 256-267.

[28] Zheng S, Yao Y, Liu D, et al. Nuclear magnetic resonance T_2 cutoffs of coals: A novel method by multifractal analysis theory[J]. Fuel. 2019, 241: 715-724.

[29] Zhao P, Wang X, Cai J, et al. Multifractal analysis of pore structure of Middle Bakken formation using low temperature N_2 adsorption and NMR measurements[J]. Journal of Petroleum Science and Engineering. 2019, 176: 312-320.

[30] Bao Y, Wang W, Ma D, et al. Gas origin and constraint of δ13C(CH_4) distribution in the Dafosi

mine field in the southern margin of the Ordos basin, China. [J]. Energy Fuels. 2020, 34(11): 14065-14073.

Table 1 Sample tests and information.

Sample No.	DP-P tests		DP-F tests	
	Information (cm)	Confine pressure (MPa)	Information (cm)	Confine pressure (MPa)
W1	2.62*2.54	5/10/15/20	1.52*2.54	10/15/20
W7	2.58*2.54	5/10/15/20	1.52*2.54	10/15/20
W9	2.60*2.54	5/10/15/20	1.52*2.54	10/15/20
W10	2.58*2.54	5/10/15/20	1.52*2.54	10/15/20

Table 2 Generalized multifractal parameters from LPN_2 GA tests.

Sample	D_{-10}	D_{10}	D_0- D_2	D_{-10}-D_0	D_0-D_{10}	D_{-10}-D_{10}
W1	0.43	1.58	0.36	0.58	0.57	1.15
W2	0.68	1.47	0.17	0.47	0.32	0.79
W3	0.68	1.51	0.17	0.51	0.32	0.83
W4	0.67	1.44	0.18	0.44	0.33	0.77
W5	0.43	1.65	0.36	0.65	0.57	1.22
W6	0.43	1.69	0.36	0.69	0.57	1.26
W7	0.43	1.63	0.36	0.63	0.57	1.20
W8	0.43	1.67	0.36	0.67	0.57	1.24
W9	0.43	1.63	0.36	0.63	0.57	1.20
W10	0.67	1.37	0.18	0.37	0.33	0.69
W11	0.67	1.46	0.18	0.46	0.33	0.78
W12	0.68	1.47	0.18	0.47	0.32	0.80

Table 3 Generalized multifractal parameters from $LPCO_2$ GA tests.

Sample No.	D_{-10}	D_{10}	D_0- D_2	D_{-10}-D_0	D_0-D_{10}	D_{-10}-D_{10}
W1	0.48	1.18	0.24	0.18	0.52	0.71
W2	0.59	1.23	0.16	0.23	0.41	0.64
W3	0.68	1.23	0.11	0.23	0.32	0.55
W4	0.67	1.21	0.13	0.21	0.33	0.54
W5	0.51	1.18	0.23	0.18	0.49	0.67

W6	0.61	1.21	0.16	0.21	0.39	0.60
W7	0.74	1.26	0.09	0.26	0.26	0.53
W8	0.48	1.20	0.25	0.20	0.52	0.72
W9	0.67	1.22	0.12	0.22	0.33	0.55
W10	0.75	1.25	0.09	0.25	0.25	0.50
W11	0.56	1.19	0.19	0.19	0.44	0.63
W12	0.61	1.21	0.16	0.21	0.39	0.61

Table 4 Diffusion coefficient variation of typical samples under different confining pressures.

Pressure (MPa)	Sample W1	Sample W7	Sample W9	Sample W10
10	2.15E-06	2.14E-06	2.41E-06	6.80E-08
15	3.45E-06	3.39E-06	2.25E-05	1.35E-07
20	4.85E-06	6.58E-06	8.89E-05	5.62E-07

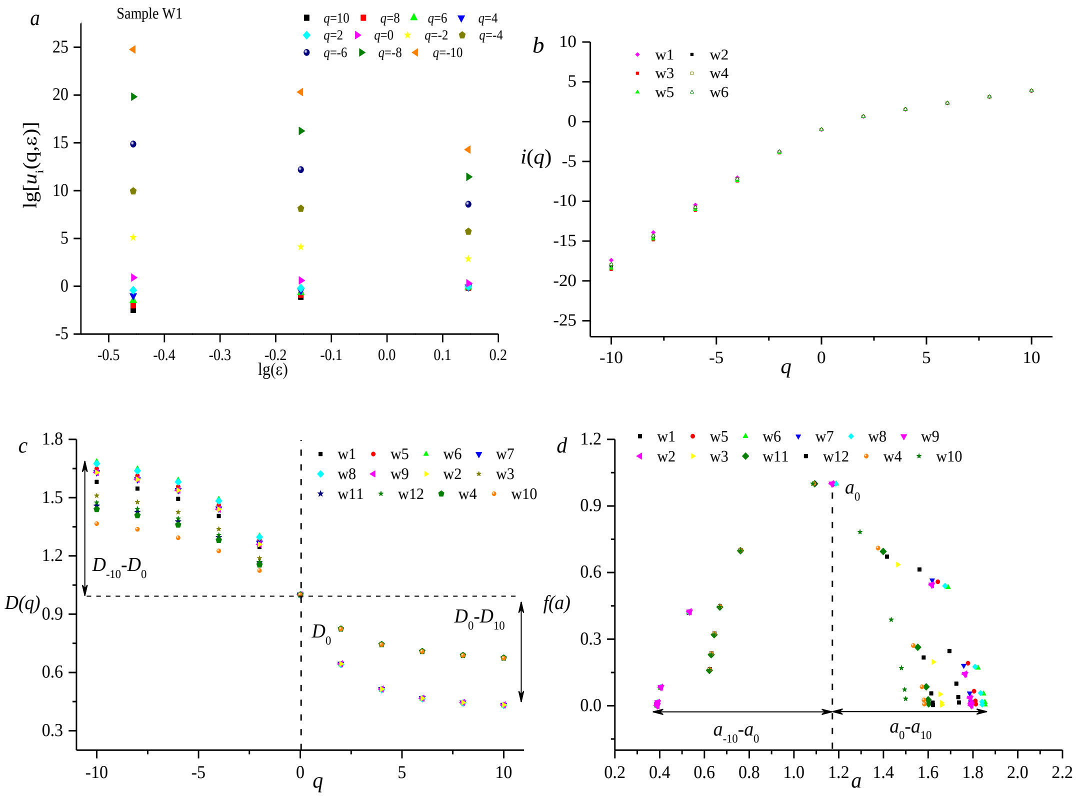

Fig.1 Characteristics of generalized multifractal curves by using LPN_2 GA tests. a, relationship between lg(ε) and lg[$u_i(q, \varepsilon)$]; b, relationship between q and $i(q)$; c, relationship between q and $D(q)$; d, relationship between a and $f(a)$.

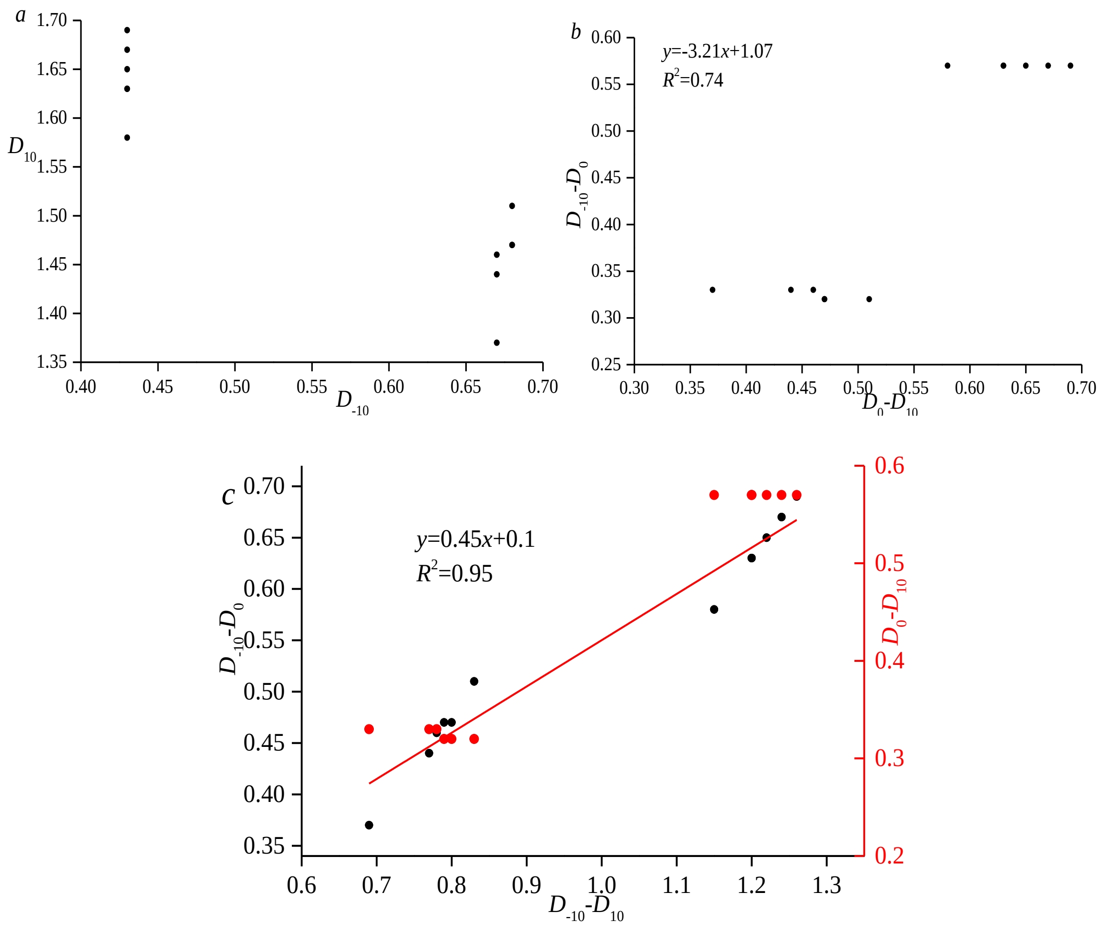

Fig. 2 Correlation analysis of generalized fractal parameters by using LPN_2 GA tests. a, relationship between D_{10} and D_{-10}; b, relationship between D_{-10}-D_0 and D_0-D_{10}; c, relationship between D_{-10}-D_{10} and D_{-10}-D_0.

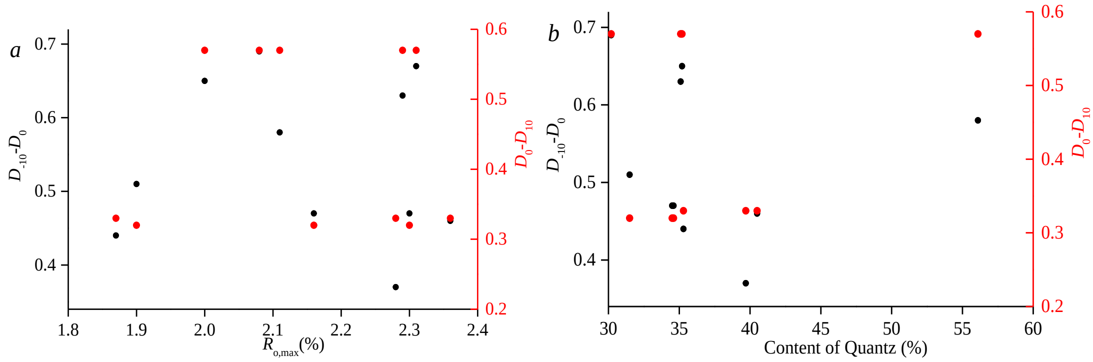

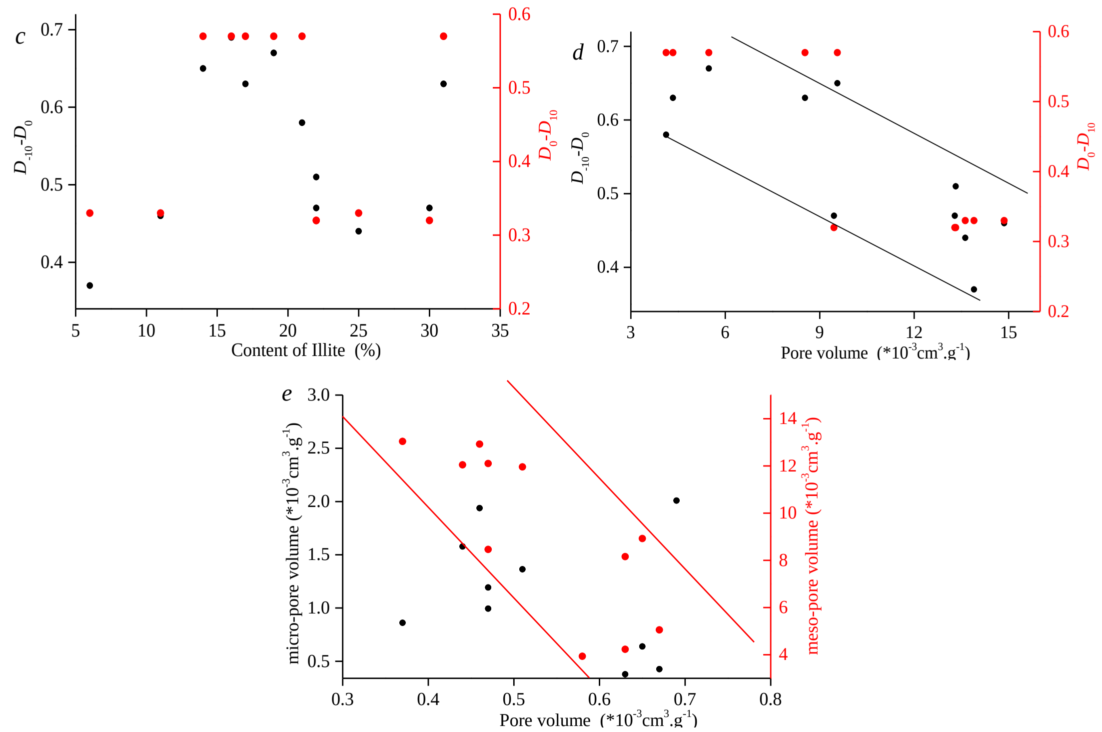

Fig. 3 Correlation analysis of generalized fractal parameters with maturity and pore structure parameters by using LPN$_2$ GA tests. a, relationship between $R_{o,\ max}$ and D_{-10}-D_0; b, relationship between quartz content and D_{-10}-D_0, D_0-D_{10}; c, relationship between illite content and D_{-10}-D_0, D_0-D_{10}; d, relationship between pore volume content and D_{-10}-D_0, D_0-D_{10}; e, relationship between pore volume content and micro-pore/meso-pore volume.

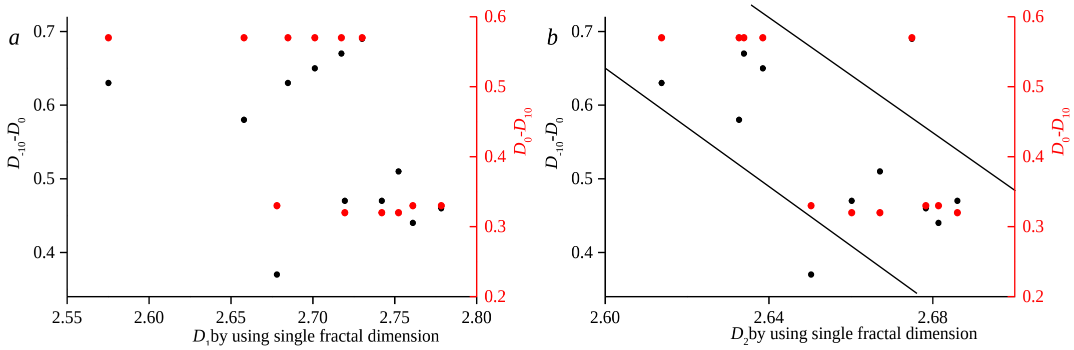

Fig. 4 Correlation analysis of fractal parameters by combining single with multifractal calculations. a, relationship between D_1 by using single fractal dimension and D_{-10}-D_0; b, relationship between D_2 by using single fractal dimension and D_0-D_{10}.

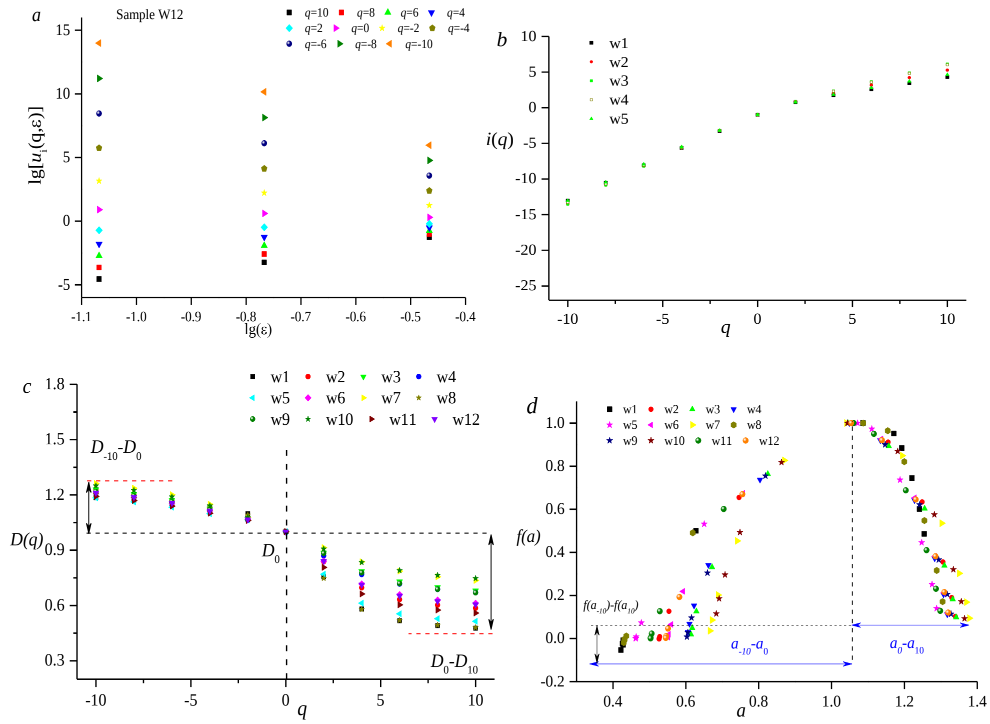

Fig. 5 Characteristics of generalized multifractal curves by using LPCO$_2$ GA tests. a, relationship between lg(ε) and lg[$u_i(q, \varepsilon)$] in sample W12; b, relationship between q and $i(q)$ of sample W12; c, relationship between q and $D(q)$ of all the samples; d, relationship between a and $f(a)$ of all the samples.

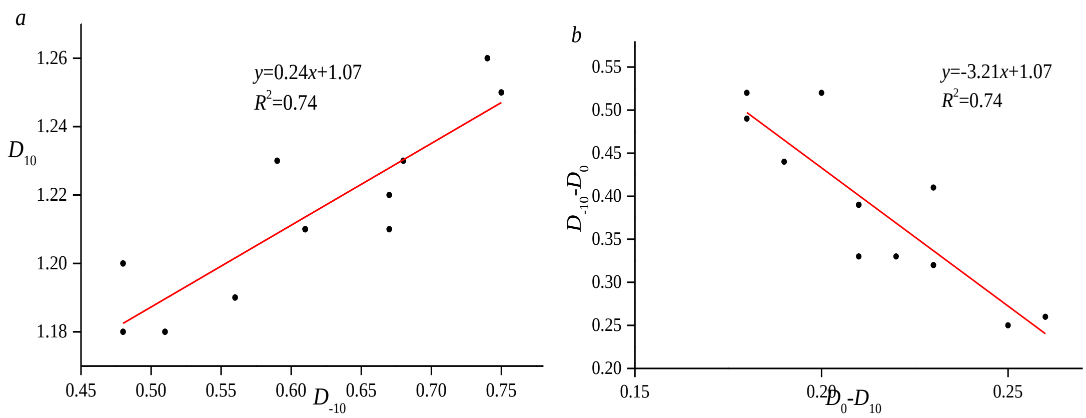

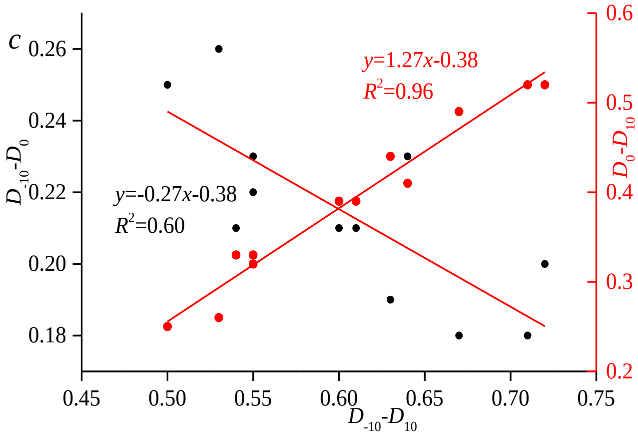

Fig. 6 Correlation analysis of generalized fractal parameters by using LPCO$_2$ GA. a, relationship between D_{10} and D_{-10}; b, relationship between D_{-10}-D_0 and D_0-D_{10}; c, relationship between D_{-10}-D_{10} and D_{-10}-D_0.

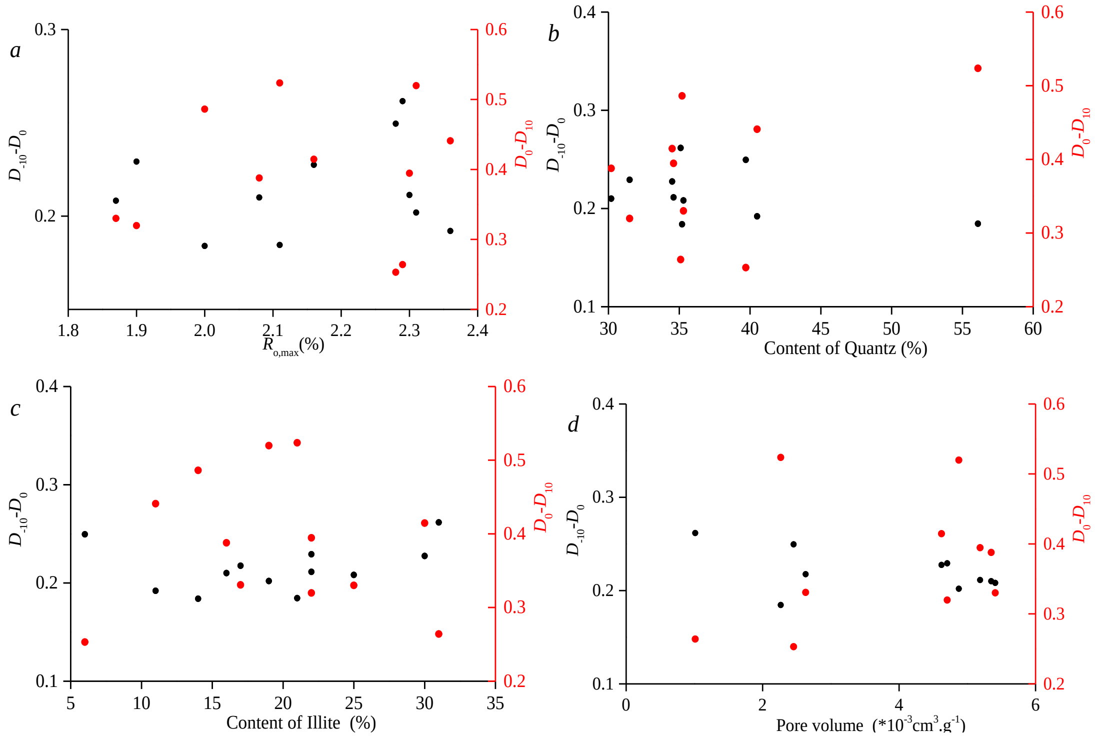

Fig. 7 Correlation analysis of generalized fractal parameters, maturity and pore structure parameters by using LPCO$_2$ GA tests. a, relationship between $R_{o,\,max}$ and D_{-10}-D_0; b, relationship between quartz content and D_{-10}-D_0, D_0-D_{10}; c, relationship between illite content and D_{-10}-D_0, D_0-D_{10}; d, relationship between pore volume content and D_{-10}-D_0, D_0-D_{10}; e, relationship between pore volume content and micro-pore/meso-pore volume.

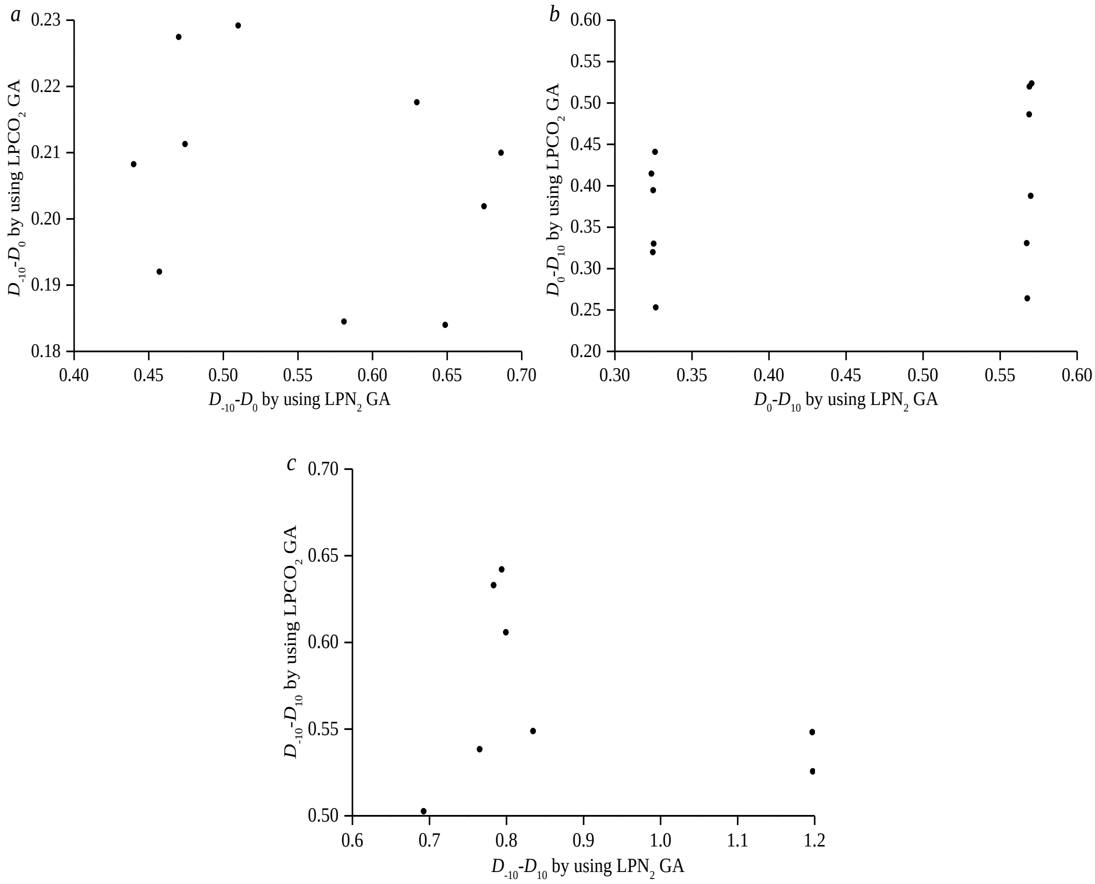

Fig.8 Correlation analysis of generalized fractal parameters by using LPCO$_2$ and N$_2$ GA tests. a, relationship between D_{-10}-D_0 by using LPCO$_2$ GA and D_{-10}-D_0 by using LPN$_2$ GA; b, relationship between D_0-D_{10} by using LPCO$_2$ GA and D_0-D_{10} by using LPN$_2$ GA; c, relationship between D_{-10}-D_{10} by using LPCO$_2$ GA and D_{-10}-D_{10} by using LPN$_2$ GA.

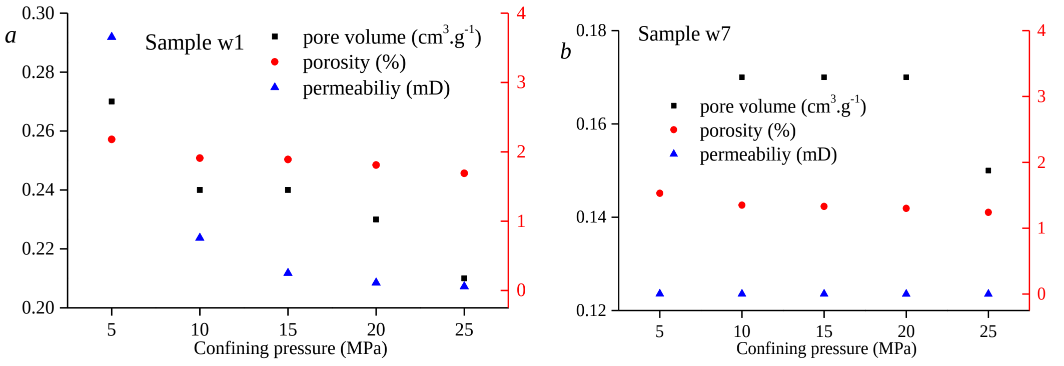

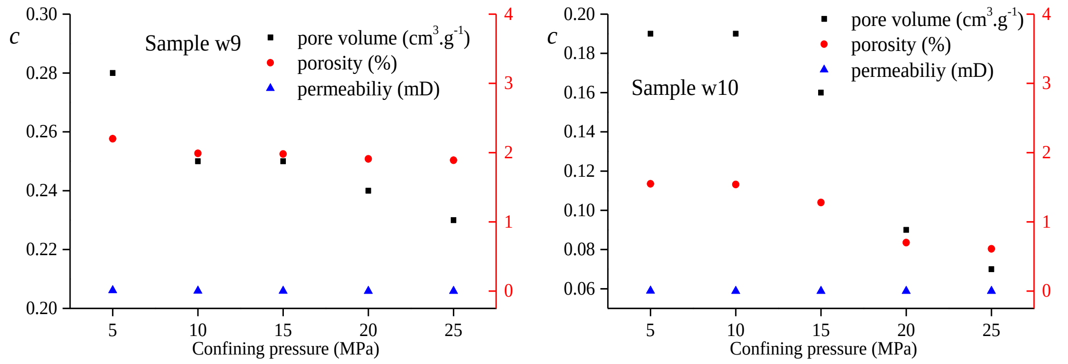

Fig. 9 Dynamic parameter variation of porosity and permeability under different confining pressures for a, sample W1; b, sample W7; c, sample W9; d, sample W10.

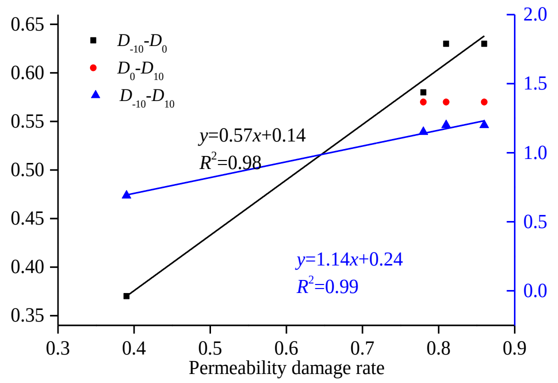

Fig. 10 The relationship between multifractal parameters and permeability damage rate based on LPN_2 GA tests.

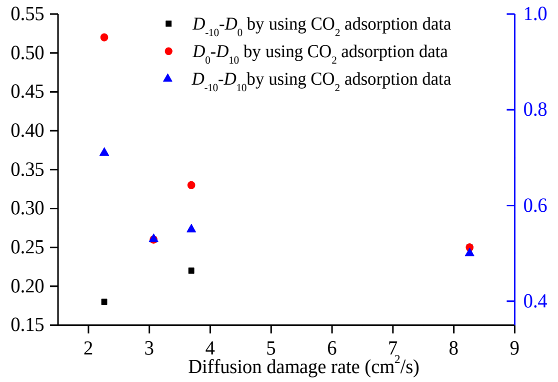

Figure 11 The relationship between multifractal parameters and damage rate of diffusion coefficient based on $LPCO_2$ GA tests.